Density Functional Studies on Dicobalt Octacarbonyl Mediated Urea Formation from Primary Amine

Fung-E. Hong* and Yu-Chang Chang

Department of Chemistry, National Chung-Hsing University, Taichung, 40227 Taiwan

Received November 11, 2003

Two adiabatic potential energy surfaces (PES) are employed for probing the process of the formation of the urea-like compound $CH_3HNC(=O)NHCH_3$, which is mediated by dicobalt octacarbonyl from the primary amine NH_2CH_3, by utilizing the density functional theory method at the B3LYP/631LAN level. These two reaction pathways described here are route 1, which is designated as an *insertion−addition* pathway, and route 2, an *addition−insertion* pathway. Elementary steps for both reaction pathways, including the amino group migration to the Co−CO bond, additional NH_2CH_3 molecule association, oxidative addition of the coordinated amine proton to the cobalt center, and reductive elimination of $-C(=O)NHCH_3$ with $-NH_2CH_3$, are modeled and examined. Rather small energies for activation ($\Delta G^{\ddagger}$), 2.3 and 2.1 kcal/mol for routes 1 and 2, respectively, are observed for the process of amino group migration and the formation of the Co−carbamyl bond in both routes. The results are in contrast to the alkyl group migration in $RCo(CO)_4$ cases, in which much higher energies are required. The oxidative addition process of the N−H bond is established as the rate-determining step (rds) for both routes, and the activation energies $\Delta G^{\ddagger}$ are 49.2 and 56.8 kcal/mol for routes 1 and 2, respectively. All the elementary steps are thermodynamically favorable, except for the oxidative addition process of the N−H bond to the cobalt center. These large energy barriers are responsible for the rigorous reaction conditions required in common transition-metal-mediated urea formation reactions and the low to medium yield in our previously reported cobalt carbonyl mediated urea-like compound formation from propargylamine. On the whole, route 2 is an energetically less favorable and more complicated reaction pathway than route 1. Furthermore, another compound, a formamide derivative, is predicted as a potential product from a competitive reaction of route 1 by our theoretical study. The process has a $\Delta G^{\ddagger}$ value smaller than that of the formation of the urea product. Nevertheless, there has been no experimental evidence for the formation of formamide until now.

Introduction

Although transition-metal-mediated carbonylation has been the object of study for a long time, the subject remains of interest to many chemists.[1] Normally, harsh reaction conditions of elevated temperature and high pressue are required when the transition metals Mn,[2] Co,[3] Ni,[4] Ru,[5] Rh,[6] W,[7] and Pd[8] are employed as catalysts. In addition to severe reaction conditions, large quantities are needed for main-group elements such as S[9] and Se[10] to be effective.

Our previous studies had demonstrated that an unusual carbonylation of primary amine took place at 25 °C, utilizing $Co_2(CO)_8$ as reaction promoter. Compound **1**, $\{[Co_2(CO)_6(\mu\text{-}HC{\equiv}C-)]CH_2NH\}_2C{=}O$, can be viewed as two propargylamine-bridged dicobalt complexes coupled by a carbonyl group through carbonyla-

* To whom correspondence should be addressed. E-mail: fehong@dragon.nchu.edu.tw.

(1) (a) Colquhoun, H. M.; Thompson, D. J.; Twigg, M. V. *Carbonylation: Direct Synthesis of Carbonyl Compounds*; Plenum: New York, 1991. (b) Sheldon, R. A. *Chemicals from Synthesis Gas*; Kluwer: Dordrecht, The Netherlands, and Boston, MA, 1983. (c) Wender, I.; Pino, P. *Organic Syntheses via Metal Carbonyls*; Wiley-Interscience: New York, 1968.

(2) (a) Dombek, B. D.; Angelici, R. J. *J. Organomet. Chem.* **1977**, *134*, 203. (b) Calderazzo, F. *Inorg. Chem.* **1965**, *4*, 293. (c) Srivastava, S. C.; Shrimal, A. K.; Srivastava, A. *J. Organomet. Chem.* **1991**, *414*, 65.

(3) (a) Bassoli, A.; Rindone, B.; Tollari, S.; Chioccara, F. *J. Mol. Catal.* **1990**, *60*, 41. (b) Leung, T. W.; Dombek, B. D. *J. Chem. Soc., Chem. Commun.* **1992**, 205. (c) Piotti, M. E.; Alper, H. *J. Am. Chem. Soc.* **1996**, *118*, 111.

(4) Giannoccaro, P.; Nobile, C. F.; Mastrorilli, P.; Ravasio, N. *J. Organomet. Chem.* **1991**, *419*, 251.

(5) (a) Mulla, S. A. R.; Rode, C. V.; Kelkar, A. A.; Gupte, S. P. *J. Mol. Catal. A: Chem.* **1997**, *122*, 103. (b) Mulla, S. A. R.; Gupte, S. P.; Chaudhari, R. V. *J. Mol. Catal.* **1991**, *67*, L7. (c) Fukuoka, S.; Chono, M.; Kohno, M. *J. Org. Chem.* **1984**, *49*, 1458.

(6) (a) Gupte, S. P.; Chaudhari, R. V. *J. Catal.* **1988**, *114*, 246. (b) Dahlen, G. M.; Sen, A. *Macromolecules* **1993**, *26*, 1784.

(7) (a) McCusker, J. E.; Grasso, C. A.; Main, A. D.; McElwee-White, L. *Org. Lett.* **1999**, *1*, 961. (b) McCusker, J. E.; Logan, J.; McElwee-White, L. *Organometallics* **1998**, *17*, 4037. (c) McCusker, J. E.; Main, A. D.; Johnson, K. S.; Grasso, C. A.; McElwee-White, L. *J. Org. Chem.* **2000**, *65*, 5216. (d) Qian, F.; McCusker, J. E.; Zhang, Y.; Main, A. D.; Chlebowski, M.; Kokka, M.; McElwee-White, L. *J. Org. Chem.* **2002**, *67*, 4086.

(8) (a) Pri-Bar, I.; Alper, H. *Can. J. Chem.* **1990**, *68*, 1544. (b) Gupte, S. P.; Chaudhari, R. V. *J. Catal.* **1988**, *114*, 246. (c) Dahlen, G. M.; Sen, A. *Macromolecules* **1993**, *26*, 1784.

(9) (a) Franz, R. A.; Applegath, F.; Morriss, F. V.; Baiocchi, F. *J. Org. Chem.* **1961**, *26*, 3306. (b) Franz, R. A.; Applegath, F.; Morriss, F. V.; Baiocchi, F.; Bolze, C. *J. Org. Chem.* **1961**, *26*, 3309.

(10) (a) Sonoda, N.; Yasuhara, T.; Kondo, K.; Ikeda, T.; Tsutsumi, S. *J. Am. Chem. Soc.* **1971**, *93*, 6344. (b) Yoshida, T.; Kambe, N.; Murai, S.; Sonoda, N. *Bull. Chem. Soc. Jpn.* **1987**, *60*, 1793. (c) Yoshida, T.; Kambe, N.; Murai, S.; Sonoda, N. *Tetrahedron Lett.* **1986**, *27*, 3037.

10.1021/om034290e CCC: $27.50
Publication on Web 01/15/2004

Scheme 1. Formation of 1

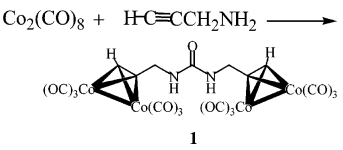

1

Scheme 2. Reaction Pathway for the Generation and Trapping of the Active Species B

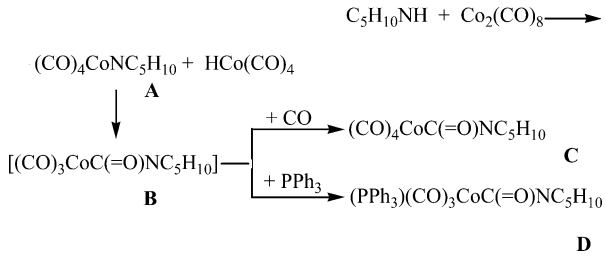

tion (Scheme 1). A reaction mechanism was proposed to account for the formation of **1**.[11]

Several closely related cases of cobalt-mediated carbonylation reactions of primary amines to give urea-like compounds were reported in the early stage of research.[12] Concerning the active metal species involved in carbonylation, Wender proposed a homomolecular disproportionation process[13] that allows the amine to activate $Co_2(CO)_8$ to a more reactive catalytic precursor, $Co(CO)_4^-$ [14] (eq 1).

$$3Co_2(CO)_8 + 12B \xrightarrow{B = \text{amines}} 2[CoB_6][Co(CO)_4]_2 + 8CO \quad (1)$$

Later, Palágyl and Markó reported that the reaction of $C_5H_{10}NH$ with $Co_2(CO)_8$ in hexane leads to a mixture of a reddish brown hexane solution plus a violet oily precipitate.[15] (Scheme 2). The hexane solution was characterized to contain variable amounts of $(CO)_4CoC(=O)NC_5H_{10}$ (**C**) and $(CO)_3(C_5H_{10}NH)CoC(=O)NC_5H_{10}$, depending on the starting $C_5H_{10}NH/Co_2(CO)_8$ molar ratio, while the oily precipitate was characterized later as the active catalytic precursor $Co(CO)_4^-$. The generally accepted reaction intermediate, $[(CO)_3CoC(=O)NC_5H_{10}]$ (**B**), for the urea-like compound formation process is not stable and is difficult to obtain in workable quantity. Nevertheless, its phosphine derivative $[(PPh_3)(CO)_3CoC(=O)NC_5H_{10}]$ (**D**) was isolated and characterized using infrared and elemental analysis by Palágyl and Markó. On the basis of the experimental observations, a reaction pathway forming $(CO)_3LCoC(=O)NC_5H_{10}$ (**C**, L = CO; **D**, L = PPh_3) was sketched and a carbamyl derivative intermediate, $(CO)_3CoC(=O)NC_5H_{10}$ (**B**), was proposed (Scheme 2). While the mechanism of Wöler's synthesis of urea has been well established by Tsipis et al.,[16] to our knowledge, a thorough computational examination of the cobalt-mediated carbonylation process of primary amine which is followed by the formation of a urea derivative has never been reported. We, therefore, start our computational studies on the $Co_2(CO)_8$-mediated carbonylation of the primary amine NH_2CH_3, from the genuine molecule, the **A**-like compound $(CO)_4CoNHCH_3$. The primary amine NH_2CH_3 was selected to replace the propargylamine-bridged dicobalt complex $Co_2(CO)_6(\mu\text{-}HC{\equiv}CCH_2NH_2)$.[11]

Since the density functional theory (DFT) method, which incorporates electron correlation effects, constantly gives reliable results on the studies of transition-metal catalytic reactions,[17] it was employed, at the B3LYP/631LAN level, to explore the process of the $Co_2(CO)_8$-mediated carbonylation of primary amine. In this study, a small amine, NH_2CH_3, was selected as the model compound to make the computational processes feasible. Two of the most probable reaction pathways for the carbonylation have been proposed and composed. They are characterized via their elementary steps as the designated *insertion*−*addition* pathway (route 1) and *addition*−*insertion* pathway (route 2). The insertion process stands for the migratory insertion of the amino group into the Co−CO bond, while the addition process represents the coordination of an additional NH_2CH_3 to the electronically unsaturated cobalt center.

Computational Methods

Ab initio screening of the cobalt-mediated carbonylation of primary amine in the formation of urea-like products has been investigated using the density functional theory method. All calculations were carried out using the Gaussian 98 package,[18] in which the tight criterion (10^{-8} hartree) is the default for the SCF convergence. To make the computations feasible, a reduced-size model compound was selected to replace the real molecule participating in the reaction. The molecular geometries were fully optimized with the hybrid B3LYP-DFT method under C_1 symmetry, in which the Becke three-parameter exchange functional[19] and the Lee−Yang−Parr correlation functional[20] were used. The LANL2DZ including the double-ζ basis sets for the valence and outermost core orbitals combined with pseudopotential were used for Co,[21,22] and 6-31G(d) basis sets were used for the other atoms. Yamanaka and Nakamura have previously employed the basis sets denoted 631LAN, which has proven successful in describing the cobalt-mediated Pauson−Khand reaction.[23] All the stationary points found were characterized via harmonic vibrational frequency analysis as minima (number of imaginary frequency $N_{imag} = 0$) and transition states ($N_{imag} = 1$). Each transition state corresponds to one reactive normal mode

(11) Hong, F. E.; Tsai, Y. T.; Chang, Y. C.; Ko, B. T. *Inorg. Chem.* **2001**, *40*, 5487.
(12) (a) Wender, I.; Sternberg, H. W.; Orchin, M. *J. Am. Chem. Soc.* **1952**, *74*, 1216−1219. (b) Natta, G.; Pino, P.; Ercoli, R. *J. Am. Chem. Soc.* **1952**, *74*, 4496−4498.
(13) Hieber, W.; Sedlmeier, J.; Abeck, W. *Chem. Ber.* **1953**, *86*, 700.
(14) Wender, I.; Sternberg, H. W.; Orchin, M. *J. Am. Chem. Soc.* **1952**, *74*, 1216−1219.
(15) Palágyl, J.; Markó, L. *J. Organomet. Chem.* **1969**, *17* 453−456.
(16) Tsipis, C. A.; Karipidis, P. A. *J. Am. Chem. Soc.* **2003**, *125*, 2307.
(17) Null, S.; Hall, M. B.; *Chem. Rev.* **2000**, *100*, 353−405.
(18) Frisch, M. J.; Trucks, G. W.; Schlegel, H. B.; Scuseria, G. E.; Robb, M. A.; Cheeseman, J. R.; Zakrzewski, V. G.; Montgomery, J. A., Jr.; Stratmann, R. E.; Burant, J. C.; Dapprich, S.; Millam, J. M.; Daniels, A. D.; Kudin, K. N.; Strain, M. C.; Farkas, O.; Tomasi, J.; Barone, V.; Cossi, M.; Cammi, R.; Mennucci, B.; Pomelli, C.; Adamo, Clifford, C.; S.; Ochterski, J.; Petersson, G. A.; Ayala, P. Y.; Cui, Q.; Morokuma, K.; Salvador, P.; Dannenberg, J. J.; Malick, D. K.; Rabuck, A. D.; Raghavachari, K.; Foresman, J. B.; Cioslowski, J.; Ortiz, J. V.; Baboul, A. G.; Stefanov, B. B.; Liu, G.; Liashenko, A.; Piskorz, P.; Komaromi, I.; Gomperts, R.; Martin, R. L.; Fox, D. J.; Keith, T.; Al-Laham, M. A.; Peng, C. Y.; Nanayakkara, A.; Challacombe, M.; Gill, P. M. W.; Johnson, B.; Chen, W.; Wong, M. W.; Andres, J. L.; Gonzalez, C.; Head-Gordon, M.; Replogle, E. S.; J. Pople, A.; *Gaussian 98*, Revision A.11; Gaussian, Inc., Pittsburgh, PA, 2001.
(19) Becke, A. D. *J. Chem. Phys.* **1993**, *98*, 5648.
(20) Lee, C.; Yang, W.; Parr, R. G. *Phys. Rev. B* **1988**, *37*, 785.
(21) Dunning, T. H., Jr.; Hay, P. J. *Modern Theoretical Chemistry*; Plenum: New York, 1976; p 1.
(22) Hay, P. J.; Wadt, W. R. *J. Chem. Phys.* **1985**, *82*, 299.
(23) Yamanaka, M.; Nakamura, E. *J. Am. Chem. Soc.* **2001**, *123*, 1703−1708.

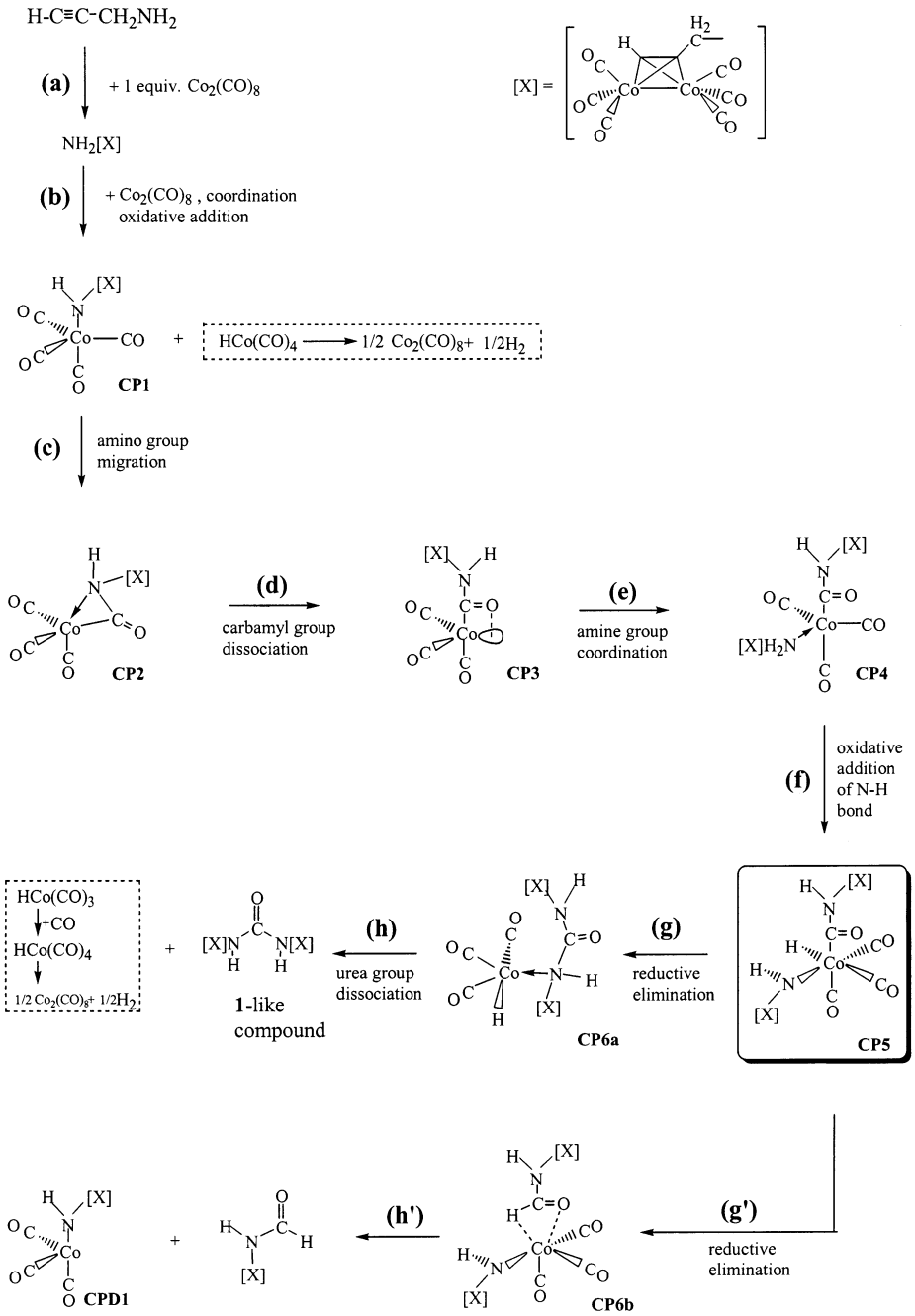

Figure 1. Formation of the urea-like product: route 1.

on the potential energy surface (PES). The analysis also provides the zero-point energy (ZPE) for each state. Thermodynamic quantities, the calculated electronic energies, the enthalpies of reaction ΔH_R, and the free activation energies$\Delta G^{\ddagger}$, were obtained and corrected at constant pressure and 298 K. Since the factor of the entropy effect cannot be overlooked in bimolecular reactions, the relative Gibbs free energies are reported throughout this paper unless otherwise stated.

For the determination of the transition-state geometry, intrinsic reaction coordinate (IRC)[24] analyses follow the geometry optimization to ensure the transition structures are smoothly connected by two proximal minima along the reaction coordinate. Stability analysis[25] has been performed to determine if the Kohn−Sham (KS) solutions are stable with respect to variations, which break spin and spatial symmetry. Localized Kohn−Sham orbitals (LOs)[26] were obtained by Boys' localization procedure from the occupied B3LYP/631LAN Kohn−Sham orbitals based on the B3LYP/631LAN optimized geometries. The wave functions were analyzed with MOLDEN[27] to plot electron density contours and visualize the IR eigenvectors.

Results and Discussion

Two of the most probable reaction routes are proposed and composed for the formation of the urea-like com-

(24) (a) Gonzalez, C.; Schlegel, H. B. *J. Chem. Phys.* **1989**, *90*, 2154. (b) Gonzalez, C.; Schlegel, H. B. *J. Phys. Chem.* **1990**, *94*, 5523.

(25) (a) Seeger, R.; Pople, J. A. *J. Chem. Phys.* **1977**, *66*, 3045−3050. (b) Bauernschmitt, R.; Ahlrichs, R. *J. Chem. Phys.* **1996**, *104*, 9047−9052.

(26) (a) Boys, S. F. In *Quantum Theory of Atoms, Molecules, and Solid State*; Lowdin, P. O., Ed.; Academic Press: New York, 1968; pp 235−262. (b) Haddon, R. C.; Williams, G. R. J. *Chem. Phys. Lett.* **1976**, *42*, 453−455. (c) Kohn, W.; Sham, L. J. *Phys. Rev.* **1965**, *140*, A1133−1138.

(27) Schaftenaar, G.; Noordik, J. H. *J. Comput.-Aided Mol. Design* **2000**, *14*, 123.

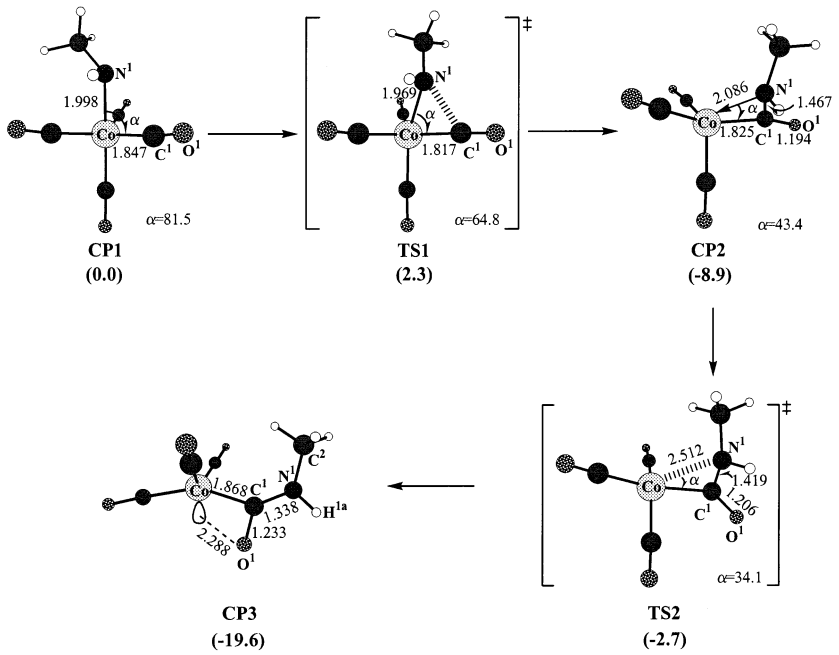

Figure 2. B3LYP/631LAN-optimized structures of stationary points involved in the processes of the migratory insertion of the $-NHCH_3$ group and the formation of the Co−carbamyl bond. Structural parameters and relative energies ΔG (kcal/mol, in parentheses) are shown. Bond lengths and bond angles are in Å and deg, respectively.

pound $CH_3HNC(=O)NHCH_3$ through cobalt-mediated carbonylation of NH_2CH_3. These two reaction pathways described here are route 1, which is designated as an insertion−addition pathway, and route 2, an addition−insertion pathway. As shown below, the two routes are basically built up by successive elementary reactions.

I. Route 1: An Insertion−Addition Pathway. Figure 1 shows the first reaction route of the $Co_2(CO)_8$-mediated carbonylation of $NH_2CH_2C{\equiv}CH$. The eight steps describing the entire route are as follows: (a) coordination of propargylamine to $Co_2(CO)_8$ and release of 2-fold carbonyls, (b) generation of $HCo(CO)_4$ and the active precursor $(CO)_4CoNH[X]$ ([X] = (μ-$HC{\equiv}CCH_2$−)$Co_2(CO)_6$), which is ready for further elementary steps, (c) migratory insertion of the $-NH[X]$ group to the Co−CO bond while maintaining the inert gas configuration of the cobalt center via the electron donation from the lone-pair electrons of nitrogen, (d) formation of the Co−carbamyl bond via the breaking of the Co−N dative bond, (e) association of an additional $NH_2[X]$ molecule, (f) N−H oxidative addition from the newly coordinated $NH_2[X]$ to the cobalt center, (g) reductive elimination of $-C(=O)NH[X]$ and $-NH[X]$ to form a urea-like derivative yet maintaining the urea−metal dative bond via one of its nitrogen atoms, and finally (h) complete dissociation of the urea-like derivative along with the active species $HCo(CO)_3$. Since the first two processes, steps a and b, are well accepted both experimentally and theoretically, our computational studies go from step c to h.[28] Theoretically, there exists another potential product, a formamide derivative, from the final reductive elimination process, step g′, of route 1; although there has been no experimental evidence observed so far. The process has an even smaller $\Delta G^{\ddagger}$ value than for the formation of the urea product.

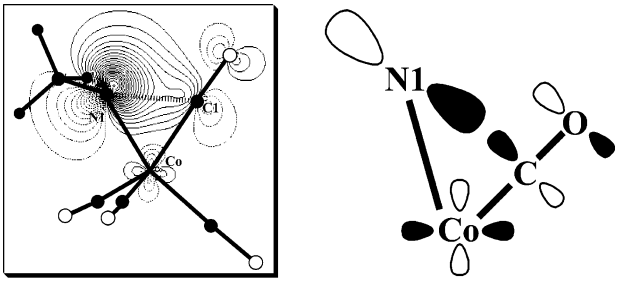

Figure 3. Localized Kohn−Sham orbital (B3LYP/6311LAN) of **TS1** in the Co−N^1−C^1 plane (contour intervals 0.025 e au^{-3}) and schematic orbital interactions.

The reduced-size model compound NH_2CH_3 has been designated to replace the alkynylamine-bridged dicobalt complex $NH_2[X]$ ([X] = (μ-$HC{\equiv}CCH_2$−)$Co_2(CO)_6$) to make the computations feasible. In step e, we did not attempt to track down the transition state of the second NH_2CH_3 association step. In each transition state, an imaginary frequency, corresponding to the active vibrational normal mode, was observed. IRC analysis following the geometry optimization also validates the connection of this transition state to its reactant and product.

1. Amino Group Migration and Carbamyl Group Formation. The geometry-optimized molecular structures from **CP1** to **CP3** are depicted in Figure 2. For **CP1**, the only located geometry on the B3LYP potential energy surface is a trigonal-bipyramidal (TBP) structure with the amino group in the axial position. As shown in Figure 1, the first crucial step of the urea formation catalytic cycle is the migratory insertion of the attached amino group to one of the coordinated carbonyls, which

(28) (a) Greenfield, H.; Sternberg, H. W.; Friedel, R. A.; Wotiz, J. H.; Markby, R.; Wender, I. *J. Am. Chem. Soc.* **1956**, *78*, 120. (b) Wido, T. M.; Young, G. H.; Wojcicki, A.; Calligaris, M.; Nardin, G. *Organometallics* **1988**, *7*, 452. (c) Berenbaum, A.; Jäkle, F.; Lough, A. J.; Manners, I. *Organometallics* **2001**, *20*, 834. (d) Blanchard, A. A.; Gilmont, P. *J. Am. Chem. Soc.* **1940**, *62*, 1192. (e) *Inorganic Syntheses*; McGraw-Hill: New York, 1946; p 238. (f) Orchin, M. *Acc. Chem. Rev.* **1981**, *14*, 259. (g) Torrent, M.; Solá, M.; Frenking, G. *Chem. Rev.* **2000**, *100*, 439−493. (h) Huo, C.-F.; Li, Y.-W.; Wu, G.-S.; Beller, M.; Jiao, H. *J. Phys. Chem. A* **2002**, *106*, 12161−12169.

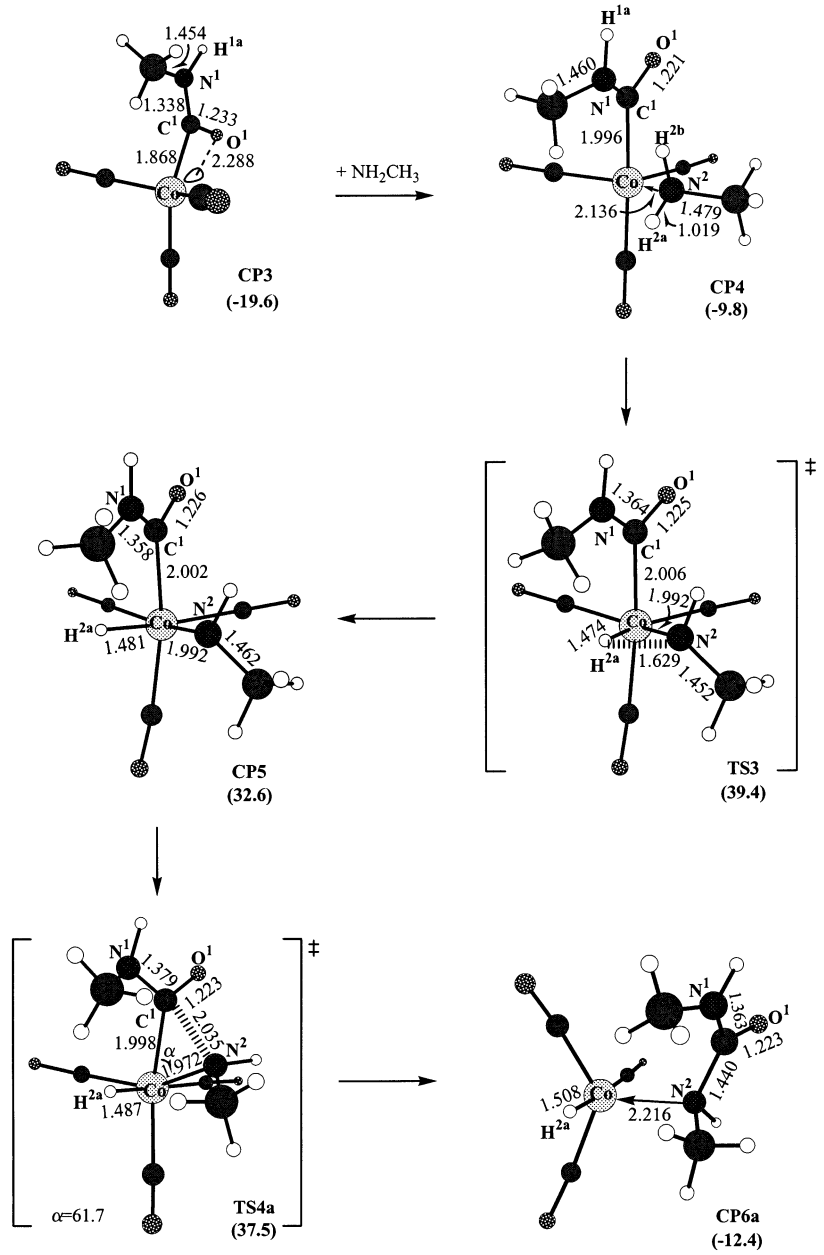

Figure 4. B3LYP/631LAN-optimized structures of stationary points involved in the processes of the amine group association, N−H oxidative addition, and reductive elimination. Structural parameters and relative energies Δ*G* (kcal/mol, in parentheses) are shown. Bond lengths and bond angles are in Å and deg, respectively.

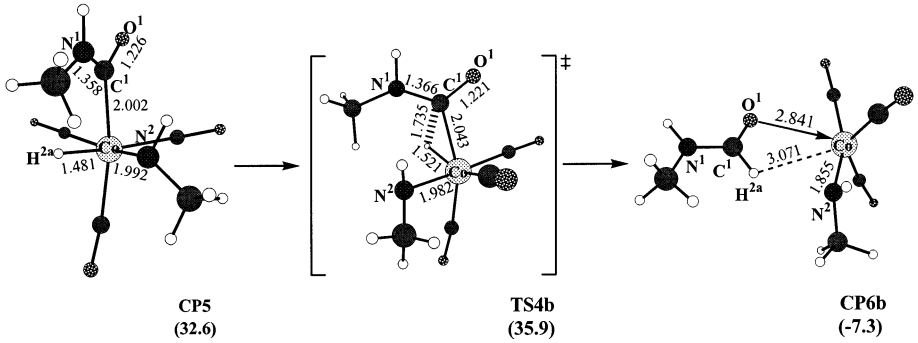

Figure 5. B3LYP/631LAN-optimized structures of stationary points involved in the processes of the hydrogen and carbamyl group reductive elimination. Structural parameters and relative energies Δ*G* (kcal/mol, in parentheses) are shown. Bond lengths and bond angles are in Å and deg, respectively.

is step c. As calculated, the free activation energy for this migratory insertion step is surprisingly low: only 2.3 kcal/mol. In contrast, the activation energy is 12 kcal/mol for the alkyl group migration in the $CH_3Co(CO)_4$ system.[29] These large activation energy differences are mainly due to the existence of an electron-

donating amino group in **CP1**. The amino group donates its lone-pair electrons to the unsaturated cobalt center, thereby maintaining the inert gas configuration of **CP2** and easing the transition, consequently lowering the activation energy. Early computational studies on the D(M−L) bond strengths in the $LCo(CO)_4$ (L = CH_3, NH_2) system had shown that the Co−CH_3 bond (38.4 kcal/mol) is stronger than the Co−NH_2 bond (35.0 kcal/mol).[30] These results are consistent with the trend of the current study.

In Figure 3, the localized Kohn−Sham orbital of **TS1** for the three-centered transition state of the dominant orbital interactions between −$NHCH_3$ and $(CO)_4$(H)Co in carbonyl insertion[31] in the Co−N^1−C^1 plane is depicted. The figure clearly shows that electron densities are dominantly donated from N^1 to the π^*_{C1-O1} orbital and a bond between N^1 and C^1 atoms is being formed.

In contrast to the alkyl group migration process, the unique feature of the amino group migration is the formation of **CP2**. It can be regarded as a cobalt complex with a pseudo-tetrahedral geometry, providing that the η^2(N,C) ligand takes one coordination site. The cobalt center maintains the inert gas configuration by accepting the electron densities donated from the lone-pair electrons of nitrogen. As shown in Figure 2, the bond length of Co−N^1 does not vary much from **CP1** (1.998 Å) to **TS1** and then to **CP2** (2.086 Å), even though substantial geometric changes are observed. Nevertheless, the distance between N^1 and C^1 atoms is narrowed down from 2.034 Å (**TS1**) to 1.467 Å (**CP2**). The latter is within the normal N−C covalent bond range. At the B3LYP level, the amino group migration process, from **CP1** to **TS1** and then to **CP2**, is calculated to be exothermic by 8.9 kcal/mol. In contrast, in the case of the alkyl group, the migratory process is always endothermic in the range of 10−20 kcal/mol.[32] Obviously, the lone-pair electrons of the amino group have played an indispensable role here in reducing the activation energy and accelerating the migration rate. From **CP2** to **TS2**, the Co−N^1 bond length is elongated from 2.086 to 2.512 Å, while the C^1−N^1 bond length does not vary much. The gradual increase in distance between the Co and N^1 atoms accounts for the Co−N^1 dative bond dissociation process from **CP2** to **TS2** and then to **CP3**. The energy required for the Co−N^1 bond-breaking process from **TS2** to **CP3**, the amino group dissociation process, is compensated by the formation of a Co−carbamyl bond. In fact, this is an exothermic process with a value of 10.7 kcal/mol. **CP3** can be regarded as an 18-electron species, providing that a dative bond from the carbamyl oxygen to the cobalt center is validated. The dihedral angle C^1−N^1−H^{1a}−C^2 of **CP3** is 179.9°. The N^1 atom is almost sp^2 hybridized. The fact that four atoms, C^1, N^1, H^{1a}, and C^2, are almost coplanar is believed to be caused by the delocalization among the lone pair of N^1 and O^1 of the carbamyl group with some correlated orbitals from the cobalt center.

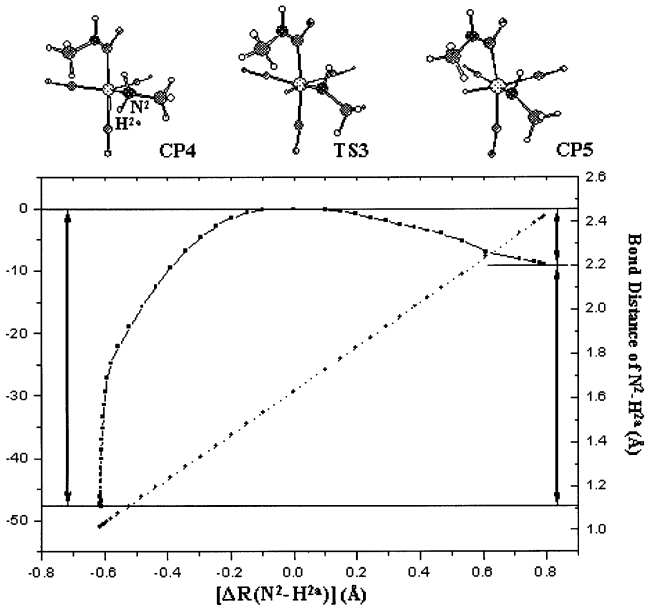

Figure 6. Reaction profile for the N−H oxidative addition, step f: relative total energies (solid line) and bond distances (dashed line) versus reaction coordinates.

2. Amine Group Association, N−H Oxidative Addition, and Reductive Elimination. The optimized molecular structures from **CP3** to **CP6a** are depicted in Figure 4. As shown in step e of Figure 1, another mole of NH_2CH_3, as an incoming group, attacks at the carbamyl group stabilized cobalt center of **CP3** at the equatorial position, forming **CP4**. **CP4** has a TBP structure with the carbamyl group in an axial position and the additive NH_2CH_3 in an equatorial position. The association of NH_2CH_3 is a thermodynamically favorable process and is endothermic by 9.8 kcal/mol. A slight increase of the Co−C^1 bond length from **CP3** (1.868 Å) to **CP4** (1.996 Å) after the coordination of NH_2CH_3 is mainly because of the donation of electron densities from the amine ligand. Along the reaction coordinate, the N−H oxidative addition process, from **CP4** to **TS3** and then to **CP5**, is found to have the highest energy barrier and is designated as the rate-determining step. The free activation energy is 49.2 kcal/mol. The N^2−H^{2a} bond length is elongated from 1.019 Å **(CP4)** to 1.629 Å **(TS3)**, while the bond length of Co−N^2 is shortened from 2.136 Å **(CP4)** to 1.992 Å **(TS3)**. The latter accounts for the change of a N^2 to Co dative bond to an electron-sharing Co−N^2 covalent bond. For **CP5**, although the reverse reaction **CP5**−**TS3**−**CP4** does not require much energy ($\Delta G^{\ddagger}$ = 6.8 kcal/mol), nevertheless, the forward reaction **CP5**−**TS4a**−**CP6a** is even more feasible ($\Delta G^{\ddagger}$ = 4.9 kcal/mol).

With **CP5** as a starting point, there is another competitive reaction route which leads to the formation of a formamide derivative product (Figures 1 and 5). The process, **CP5**−**TS4b**−**CP6b**, has a smaller $\Delta G^{\ddagger}$ value than the process of forming the urea derivative product (i.e., 3.3 and 4.9 kcal/mol, respectively). As presented in Figure 5, the Co−H^{2a} bond length is elongated from 1.481 Å **(CP5)** to 1.521 Å **(TS4b)** and the bond length of Co−C^1 is elongated from 2.002 Å **(CP4)** to 2.043 Å (**TS4b**). On the other hand, the gradual formation of

(29) Goh, S. K.; Marynick, D. S. *Organometallics* **2002**, *21*, 2262−2267.
(30) Ziegler, T.; Tschinke, V.; Versluis, L. *Polyhedron* **1988**, *7*, 1625−1637.
(31) Koga, N.; Morokuma, K. *Chem. Rev.* **1991**, *91*, 823−842.
(32) (a) Salem, L. In *Electrons in Chemical Reactions*; Wiley: New York, **1982**. (b) Komornicki, A., McIver, J. W. *J. Am. Chem. Soc.* **1974**, *96*, 5798. (c) Torrent, M.; Solá, M.; Frenking, G. *Chem. Rev.* **2000**, *100*, 439−493.

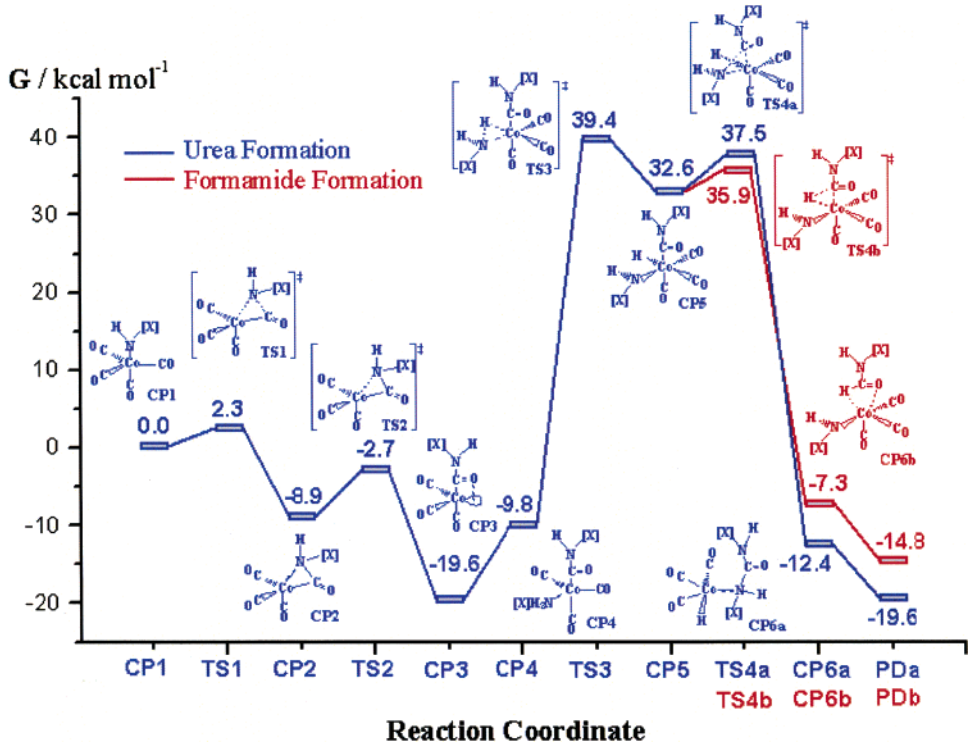

Figure 7. Free energies of states involved in the route 1 course of cobalt-mediated carbonylation of NH_2CH_3. Free energies (kcal/mol) were calculated at the B3LYP/631LAN level of theory.

the C^1-H^{2a} covalent bond (1.735 Å) is described in the geometry of **TS4b**. **CP6b** is shown to be a supermolecule composed of a formamide derivative and a $CH_3NHCo(CO)_3$ fragment. The largely shortened $Co-N^2$ bond distance shows that more electron density is donated from N^2 to the electron-deficient cobalt center. Although predicted by the theroretical study as a potential product, there has been no experimental evidence so far for the formation of the expected formamide derivative product.

The whole N−H oxidative addition process, **CP4**−**TS3**−**CP5**, has been monitored by means of the intrinsic reaction coordinate (IRC) calculations at the B3LYP/631LAN level. A plot for the process with small variations of reaction coordinate ($\Delta R(N^2-H^{2a})$) vs relative energies is sketched. In Figure 6, the transition structure **TS3** is assigned to zero (at the center) on the reaction coordinate, with the reactant **CP4** on the left at the local minimum and the product **CP5** on the right at another local minimum. Results from the reaction profile analyses have shown that the N^2-H^{2a} bond distance increases in a linear manner and have proven that the transition structure **TS2** is smoothly connected with the reactant **CP4** and the product **CP5** and that no other local minimum exists.

The optimized geometry of **CP5** reveals that it is a distorted octahedron with the carbamyl group and the amino group being arranged in cis positions. Similarly, the geometry of **TS4a** shows that $\angle C^1-Co-N^2 = 61.7°$, which is beneficial to the later reductive elimination of these two groups. The structure also indicates the formation of the N^2-C^1 σ bond and the N^2-Co dative bond and, at the same time, breaking of the $Co-C^1$ bond. **CP6a** can be viewed as a urea-like compound, a $CH_3HNC(=O)NHCH_3$-coordinated cobalt complex. The reductive elimination process is the most exothermic step by 45.0 kcal/mol. The last step, step g, is the dissociation of the urea-like product from the active $HCo(CO)_3$ fragment. The dissociation process is exothermic by 7.2 kcal/mol. The dissociated urea-like product, $CH_3HNC(=O)NHCH_3$, has yet to be transformed to its lowest energetic conformer with the two substituents on the side of the carbonyl.[11,33] The dissociated $HCo(CO)_3$ species from the process is in its singlet ground state with C_{2v} symmetry and has hydrogen in the axial position. This observation is in accord with the latest density functional studies by Jiao et al.;[28h] nevertheless, it differs from a reported C_s symmetry found earlier by Ziegler's density functional studies with local density approximation.[34] Subsequently, the active $HCo(CO)_3$ is ready to pick up one CO from the environment and form $HCo(CO)_4$. Finally, two $HCo(CO)_4$ molecules react disproportionately to give $Co_2(CO)_8$ and H_2.[35] The cobalt compound might re-enter the reaction cycle.

3. Potential Energy Surface of Route 1. In Figure 7, the entire potential energy surface of route 1 is presented. It is constructed from each of the corresponding elementary steps discussed above. The free activation energies ($\Delta G^{\ddagger}$) as well as the imaginary frequencies of the matching transition states are also listed in Table 1. It is clearly seen that the N−H oxidative addition process, **CP4**−**TS3**−**CP5**, is the most endothermic step and the reductive elimination process, **CP5**−**TS4a**−**CP6a**, is the most exothermic step. The whole process is thermodynamically favorable by 19.6 kcal/mol.

(33) Masunov, A.; Dannenberg, J. J. *J. Phys. Chem. A* **1999**, *103*, 178−184.
(34) Ziegler, T.; Cavallo, L.; Bérces, A. *Organometallics* **1993**, *12*, 3586.
(35) Wener, I.; Greenfield, H.; Metlin, S.; Orchin, M. *J. Am. Chem. Soc.* **1952**, *74*, 4079−4083.

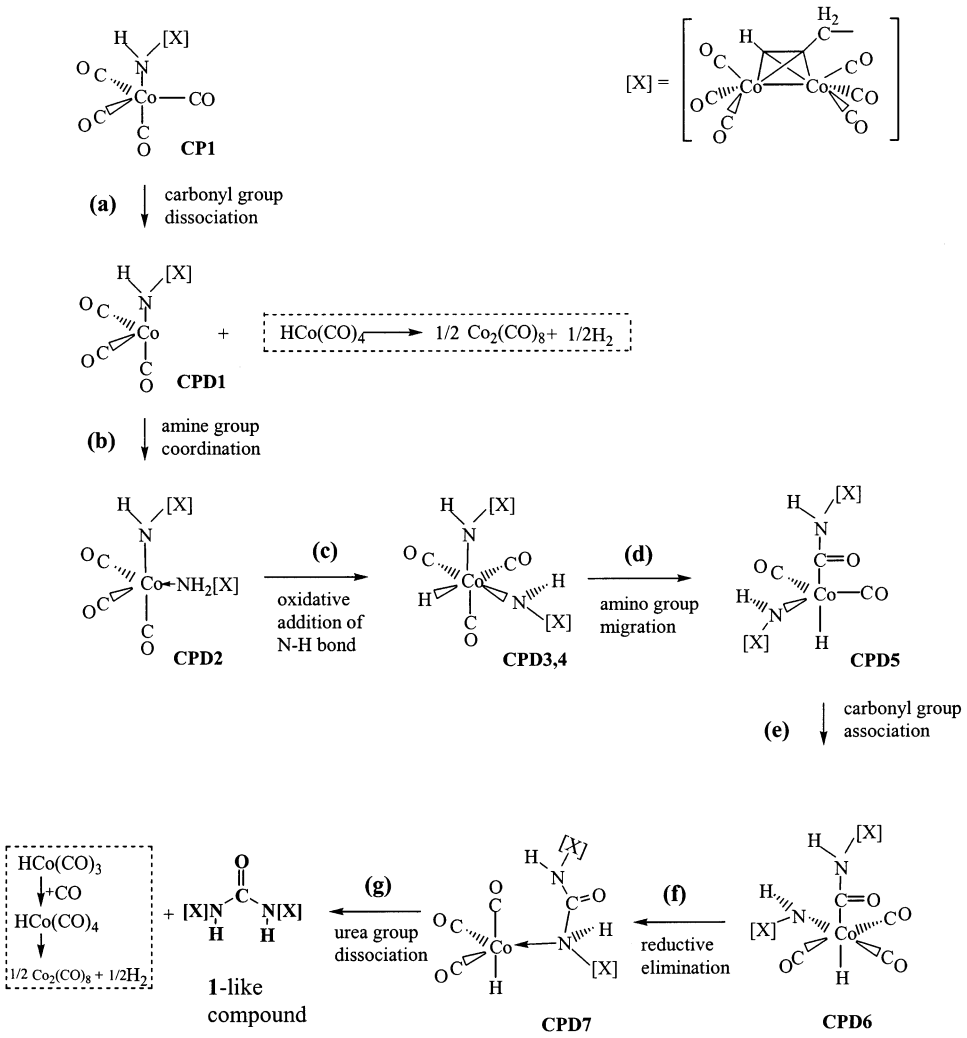

Figure 8. Formation of urea-like product: route 2.

Table 1. Imaginary Frequencies and Free Activation Energies for the Matching Transition States of Route 1

saddle point	$\Delta G^{\ddagger}$ (kcal/mol)	freq (cm^{-1})
TS1	2.3	154*i*
TS2	6.2	147*i*
TS3	49.2	1032*i*
TS4a	4.9	210*i*
TS4b	3.3	550*i*

II. Route 2: An Addition−Insertion Pathway. An alternative reaction pathway for urea-like derivative formation reaction is designated as the addition−insertion pathway. Figure 8 shows the second reaction course of the $Co_2(CO)_8$-mediated carbonylation of NH_2-$CH_2C{\equiv}CH$. In contrast to route 1, our studies on route 2, the addition−insertion pathway, starts from **CPD1**. The unsaturated compound **CPD1** might be obtained from a CO-released **CP1.** The whole reaction course includes the following elementary steps: (a) dissociation of one of the carbonyls from $(CO)_4CoNH[X]$ and generation of an unsaturated intermediate, $[X]NHCo(CO)_3$, (b) association of an additional $NH_2[X]$ molecule and generation of the coordinatively saturated intermediate $[X]$-$NHCo(CO)_3NH_2[X]$, (c) N−H oxidative addition from the coordinated amine ligand to the cobalt center, (d) migratory insertion of the −NH[X] group into the Co−CO bond, (e) carbonyl group association, (f) reductive elimination of −C(═O)NH[X] and −NH[X] and formation of a urea-coordinated cobalt compound, and (g) dissociation of the urea-like compound from the active $HCo(CO)_3$. Since **CP1** has been well studied in route 1, our computational studies started from **CPD1**, a CO-released **CP1.** It is worth noting that a small rotation of the Co−N bond from **CPD3** to **CPD4** is essential, even though it has negligible activation free energy (1.8 kcal/mol), before step d can be pursued further.

1. Amine Group Addition and N−H Oxidative Addition. The geometry-optimized molecular structures from **CP1** to **CPD3** are depicted in Figure 9. As proposed in route 2, the coordinative unsaturated intermediate **CPD1**, with one CO ligand librated from **CP1**, has to be formed before the formation of **CPD2**, via the coordination of another amine ligand. As shown in Figure 9, **TSa** represents the transition state of the dissociation process. One of the carbonyls from the equatorial position of **CP1** is released with surprisingly low activation energy: 5.9 kcal/mol. Again, the electron-donating amino group in **CP1** must play an important role in smoothing the transition by way of donating its lone-pair electrons to the unsaturated cobalt center, thereby lowering the free activation energy. This is also evidenced by the fact that the shortening of the Co−N^1 bond length, from 1.998 Å (**CP1**) to 1.811 Å (**CPD1**), is observed. Accordingly, the shorter bond length of Co−

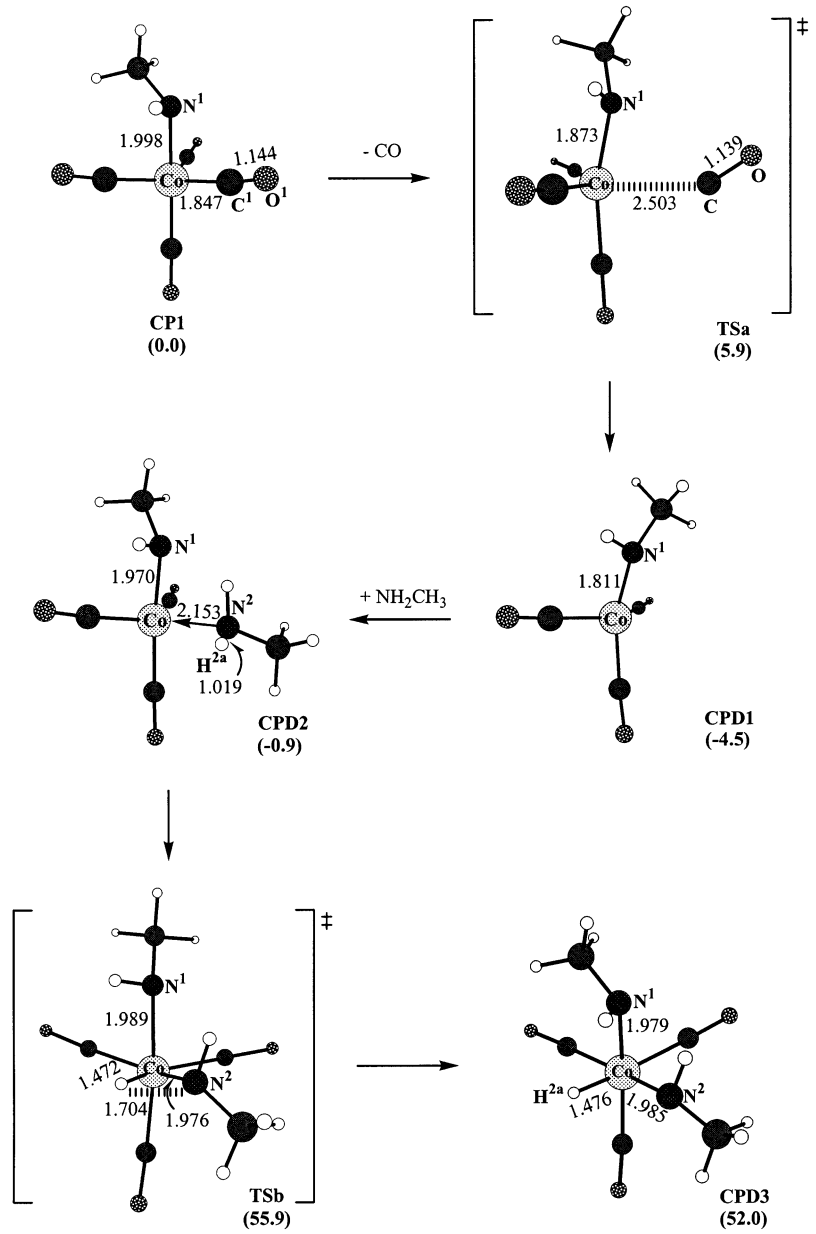

Figure 9. B3LYP/631LAN-optimized stationary points involved in the processes of the amine group addition and N−H oxidative addition. Structural parameters and relative energies ΔG (kcal/mol, in parentheses) are shown. Bond lengths and bond angles are in Å and deg, respectively.

N^1 also reveals that more electron density is donated from N^1 to the electron-deficient cobalt center. The elongation of the Co−CO bond length from 1.847 Å (**CP1**) to 2.503 Å (**TSa**) will finally lead to the dissociation of the equatorial CO. The coordination of an additional NH_2CH_3 to the unsaturated intermediate **CPD1** leads to the formation of the less stable compound **CPD2** by 3.6 kcal/mol. Subsequently, the N−H oxidative addition process, from **CPD2** to **TSb** and then to **CPD3**, takes place. The process is found to have the highest energy barrier (56.8 kcal/mol) along the reaction course and is designated as the rate-determining step. Meanwhile, notable geometric changes, from TBP (**CPD2**) to O_h (**CPD3**), are observed. A large elongation of the N^2-H^{2a} bond length is found on going from **CPD2** to **TSb**, stretching from 1.019 to 1.704 Å, respectively. This large variation (i.e. 0.685 Å) in bond length leads to the breaking of the N^2-H^{2a} bond later in **CPD3**.

The whole N−H oxidative addition process, **CPD2**−**TSb**−**CPD3**, is monitored by means of IRC calculations at the B3LYP/631LAN level. A plot for the process with small variations of $\Delta R(N^2-H^{2a})$ vs relative energies is sketched. In Figure 10, the transition structure **TSb** is assigned to zero (at the center) on the reaction coordinate with the reactant, **CPD2**, on the left at the local minimum and the product, **CPD3**, on the right at another local minimum. Results from the reaction profile have shown that the N^2-H^{2a} bond distance increases in a linear manner and that **TSb** is the transition state between **CPD2** and **CPD3**.

Interestingly, a proper interrelated orientation of two amino groups in **CPD3** is crucial for locating the transition state **TSd** of the amino group migratory insertion process. In fact, this orientation can be easily achieved by rotation of the Co−$NHCH_3$ bond to an appropriate position. This process, from **CPD3** to **TSc**

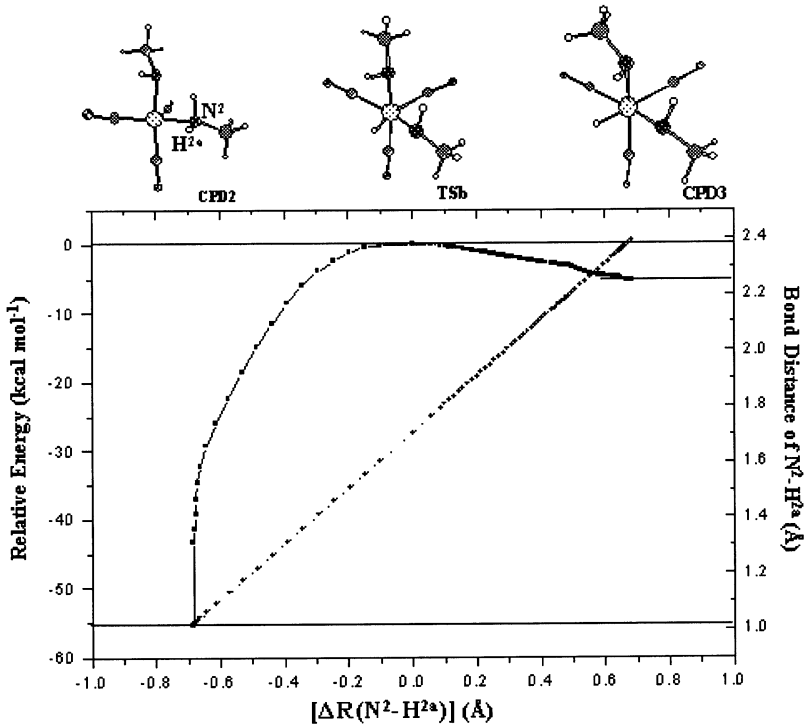

Figure 10. Reaction profile for the N−H oxidative addition, step c: relative total energies (solid line) and bond distances (dashed line) versus reaction coordinates.

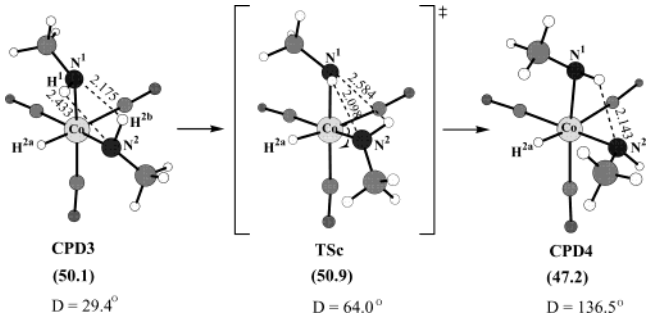

Figure 11. B3LYP/631LAN-optimized stationary points of the Co−N bond rotation process. Structural parameters and relative energies ΔG (kcal/mol, in parentheses) are shown. Bond lengths and bond angles are in Å and deg, respectively. Dihedral angles (D) of N^1−Co−N^2−H^{2b} are in deg.

and then to **CPD4**, is carried out with a negligible energy barrier (1.8 kcal/mol) (Figure 11). Presumably, two factors might be involved to hinder the amino group migratory insertion process: first, intramolecular hydrogen bonding between two amino groups locks the movement of the amino group (the bond lengths of $N^1\cdots N^2$, $N^1\cdots H^{2b}$, and $N^2\cdots H^1$ are 2.572, 2.175, and 2.433 Å, respectively), although these optimized parameters do not indicate a strong interaction;[36] second, one of the amino protons blocks the way of the migratory insertion process.

2. Amino Group Migration, Carbonyl Group Association, and Reductive Elimination. The optimized molecular structures from **CPD4** to **CPD7** are depicted in Figure 13. All these steps mentioned here are thermodynamically favorable processes. Once **CPD4** is formed, the migratory insertion process, from **CPD4**

(36) Jeffrey, G. A.; Saenger, W. *Hydrogen Bond in Biological Systems*; Springer: Berlin, 1991.

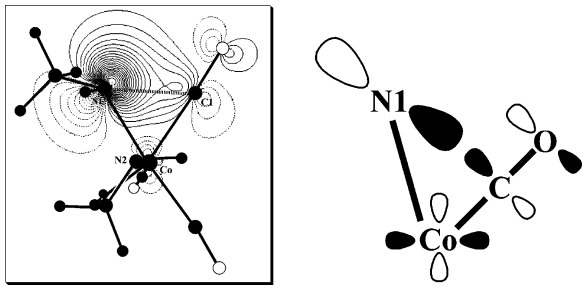

Figure 12. Localized Kohn−Sham orbital (B3LYP/6311LAN) of **TSd** in the Co−N^1−C^1 plane (contour intervals 0.025 e au^{-3}) and schematic orbital interactions.

to **TSd** and then to **CPD5**, can proceed readily through the transition state, **TSd**, with a rather small energy barrier ($\Delta G^{\ddagger} = 2.1$ kcal/mol). We observed that the N^1−C^1 bond distance/length is shortened from 2.070 to 1.371 Å for **TSd** to **CPD5**, respectively. This large variation (i.e. 0.699 Å) in bond length leads to the formation of the C^1−N^1 bond in **CPD5**. Meanwhile, the structure changes from O_h for **TSd** to TBP for **CPD5**. It is worth noting that the position of the hydride changes from the equatorial position of O_h in **CPD4** to the axial position of TBP in **CPD5**, and the bond length Co−H^{2a} is slightly elongated by 0.08 Å. Compared with the corresponding migratory insertion process, that is **CP1**−**TS1**−**CP2**−**TS2**−**CP3** in route 1, there is no matching **CP2**-like structure, a η^2(N,C)-coordinated 18-electron species, and **CP3**-like structure, a η^2-acyl coordinated 18-electron species, that can be located here in route 2. To achieve the noble gas configuration of **CPD6**, one carbonyl group has to be picked up from the environment by the electron-unsaturated **CPD5**. The incoming carbonyl attacks **CPD5** from the equatorial position and forms **TSe** with a small energy barrier (2.8 kcal/mol), which later leads to **CPD6**. We may note, in passing, that the

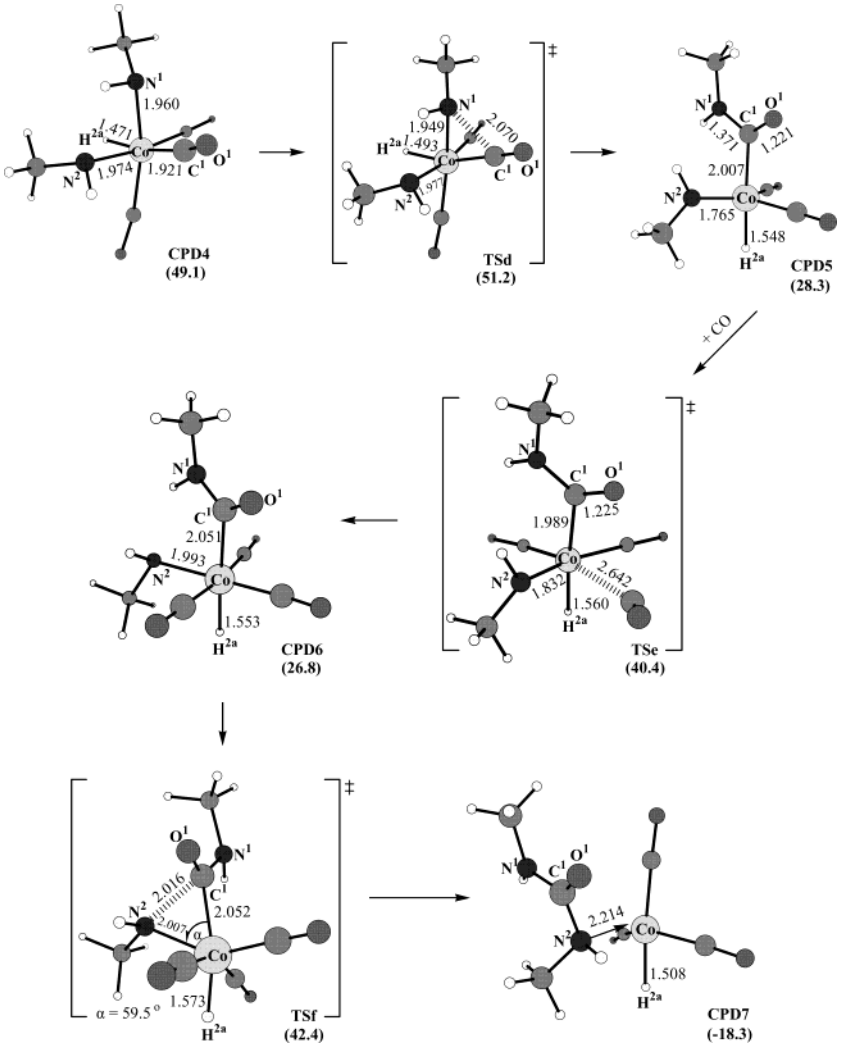

Figure 13. B3LYP/631LAN-optimized stationary points involved in the processes of the amino group migration, carbonyl group association, and reductive elimination. Structural parameters and relative energies ΔG (kcal/mol, in parentheses) are shown. Bond lengths and bond angles are in Å and deg, respectively.

hydride takes cis and trans positions for **CP5** in route 1 and **CPD6** in route 2, respectively, with respect to the carbamyl group. This is believed to be caused by the intrinsic nature of the reaction pathways rather than the stabilities of various conformers. Subsequently, the process of reductive elimination, that is from **CPD6** to **TSf** and then to **CPD7**, is exothermic (45.1 kcal/mol) with an energy barrier of 15.6 kcal/mol. In comparison with the corresponding step in route 1 (**CP5**−**TS4a**−**CP6a**: $\Delta G^{\ddagger} = 4.9$ kcal/mol), the process takes much higher energy to overcome the reaction barrier and, at the same time, releases more energy. Again, **CPD7** can be viewed as a urea-like compound, a $CH_3HNC(=O)$-$NHCH_3$-coordinated cobalt complex. The last step, step g, is the dissociation of the urea-like product from the active $HCo(CO)_3$ fragment. The dissociation process is exothermic by 6.1 kcal/mol, the same as the corresponding step in route 1.

In Figure 12, the localized Kohn−Sham orbital of **TSd** for the three-centered transition state of the dominant orbital interactions between $-NHCH_3$ and $(CO)_3(H)$-$CoNHCH_3$ in carbonyl insertion in the Co−N^1−C^1 plane is depicted.

3. Potential Energy Surface of Route 2. In Figure 14 is shown the entire potential energy surface of route 2. The free activation energies as well as the imaginary frequencies of the matching transition states are also listed in Table 2. It is clearly seen that the N−H oxidative addition process, **CPD2**−**TSb**−**CPD3**, is the most endothermic step and the reductive elimination process, **CPD6**−**TSf**−**CPD7**, is the most exothermic step. Along the PES of route 2, a simple yet crucial problem of locating the proper interrelated orientation of the two amino groups has to be resolved before the migratory insertion and further steps can be pursued (Figure 14). Fortunately, the transition structure **TSc** was located with the corresponding vibrational mode and one small imaginary frequency, 52*i* cm^{-1}. Note that in route 2, there is no matching reaction route for the formation of a formamide derivative product as depicted in route 1. This is because of the fact that the hydride

Table 2. Imaginary Frequencies and Activation Energies for the Matching Transition States of Route 2

saddle point	$\Delta G^{\ddagger}$ (kcal/mol)	freq (cm^{-1})
TSa	5.9	120*i*
TSb	56.8	925*i*
TSc	1.8	52*i*
TSd	2.1	144*i*
TSe	12.1	123*i*
TSf	15.6	257*i*

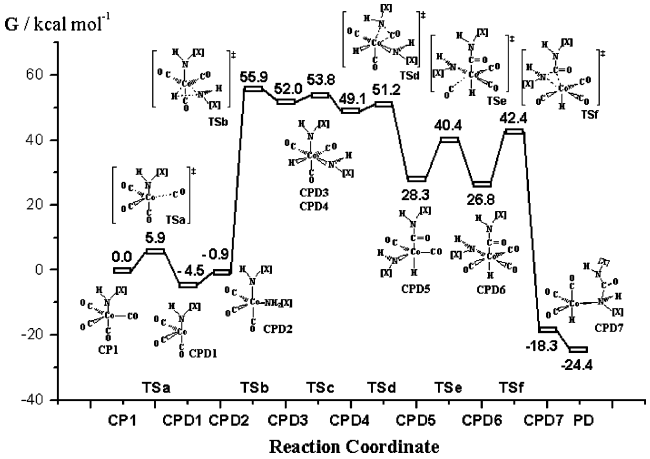

Figure 14. Energies of states involved in the route 2 course of cobalt-mediated carbonylation of NH_2CH_3. Energies (kcal/mol) were calculated at the B3LYP/631LAN level of theory.

and the carbamyl group are in trans positions, which eradicates the possibility of a reductive elimination process. Generally speaking, route 2 is energetically less favorable and more complicated than route 1.

Summary

We have explored the reaction pathways of the $Co_2(CO)_8$-mediated carbonylation of the primary amine NH_2CH_3. Two alternative reaction pathways, route 1 (insertion−addition pathway) and route 2 (addition−insertion pathway), are proposed and examined, utilizing the density functional theory method at the B3LYP/631LAN level. The N−H oxidative addition process is found as the rate-determining step (rds) for both routes, and the activation energies are 49.2 and 56.8 kcal/mol for routes 1 and 2, respectively. These large energy barriers are responsible for the rigorous reaction conditions required in cobalt-mediated urea formation reaction. The reductive elimination process is found to be the most exothermic process for both routes. This DFT study also predicts the formation of a formamide derivative compound as a competitive potential product in addition to the formation of the urea compound from route 1. To our knowledge, this is the first integrated computational examination for the $Co_2(CO)_8$-mediated carbonylation of a primary amine. In principle, the conclusion from this study should extend to other $Co_2(CO)_8$-mediated/catalytic urea formation from various primary or secondary amines.

Acknowledgment. We thank the National Science Council of the ROC (Grant No. NSC-91-2113-M-005-017) for financial support. The CPU time that was used to complete this project was partially provided by the National Center for High-Performance Computing (NCHC). We are also grateful to Dr. Dirk V. Deubel, Dr. Masahiro Yamanaka, and Mr. Chen-Chang Wu for some important technical discussions.

Supporting Information Available: Tables containing coordinates and energies of the optimized stationary points. This material is available free of charge via the Internet at http://pubs.acs.org.

OM034290E